Cover Letter for

First Observations of a Foreshock Bubble at Earth: Implications for Magnetospheric Activity and Energetic Particle Acceleration

D. L. Turner[1], N. Omidi[2], D. G. Sibeck[3], and V. Angelopoulos[1]

[1] University of California, Los Angeles, CA, USA
[2]Solana Scientific Inc., Solana Beach, CA, USA
[3]NASA Goddard Space Flight Center, Greenbelt, MD, USA

Correspondence to: drew.lawson.turner@gmail.com

Summary Statement: Here we present unprecedented, multi-point observations of a recently predicted astrophysical plasma phenomenon, foreshock bubbles, which have not been identified previously *in situ*. We discuss the event's global effects on the magnetosphere and the energetic ions and electrons accelerated in the foreshock bubble, potentially by a combination of first and second order Fermi and shock drift acceleration processes. This new phenomena should play a role in energetic particle acceleration at collisionless, quasi-parallel shocks throughout the Universe.

Thank you for your time in reviewing this manuscript.

Colleagues who have reviewed this paper:
None

First Observations of a Foreshock Bubble at Earth: Implications for Magnetospheric Activity and Energetic Particle Acceleration

D. L. Turner[1*], N. Omidi[2], D. G. Sibeck[4], and V. Angelopoulos[1,4]

[1] Institute of Geophysics and Planetary Physics, University of California, Los Angeles, CA, USA

[2] Solana Scientific Inc., Solana Beach, CA, USA

[3] NASA Goddard Space Flight Center, Greenbelt, MD, USA

[4] Department of Earth and Space Sciences, University of California, Los Angeles, CA, USA

[*] Corresponding author; correspondence to: drew.lawson.turner@gmail.com

Summary Sentence: Here we present unprecedented, multi-point observations of a recently predicted astrophysical plasma phenomenon, foreshock bubbles, which should play a role in energetic particle acceleration at collisionless, quasi-parallel shocks throughout the Universe.

Abstract: **Earth's foreshock, which is the quasi-parallel region upstream of the bow shock, is a unique plasma region capable of generating several kinds of large-scale phenomena, each of which can impact the magnetosphere resulting in global effects. Interestingly, such phenomena have also been observed at planetary foreshocks throughout our solar system. Recently, a new type of foreshock phenomena has been predicted: foreshock bubbles, which are large-scale disruptions of both the foreshock and incident solar wind plasmas that can result in global magnetospheric disturbances. Here we present unprecedented, multi-point observations of foreshock bubbles at Earth using a combination of spacecraft and ground observations primarily from the Time History of Events and Macroscale Interactions during Substorms (THEMIS) mission, and we include detailed analysis of the events' global effects on the magnetosphere and the energetic ions and electrons accelerated by them, potentially by a combination of first and second order Fermi and shock drift acceleration processes. This new phenomena should play a role in energetic particle acceleration at collisionless, quasi-parallel shocks throughout the Universe.**

Because the solar wind at one astronomical unit is super-magnetosonic, i.e., faster than both the ion acoustic and Alfvén speeds, a bow shock forms as the plasma is deflected, heated, and slowed to pass around Earth's magnetosphere, the cavity produced by the planet's magnetic field. Like other collisionless astrophysical shocks, Earth's bow shock is an effective accelerator of energetic particles via shock drift and/or Fermi acceleration processes ([Scholer et al., 1998], [Giacalone, 1992]). When the interplanetary magnetic field (IMF) is quasi-parallel to the bow shock, energetic ions and electrons accelerated and

reflected at the shock travel back upstream along magnetic field lines. These hot, backstreaming particles create instabilities within the incident solar wind plasma, generating waves that result in additional particle scattering. This upstream region of energetic ions and waves is known as the ion foreshock ([Fuselier, 1995]). The thermal pressure in the foreshock is enhanced, which results in compression regions forming along its boundaries; this boundary region of enhanced magnetic field and density is known as the foreshock compressional boundary ([Sibeck et al., 2008]). However, the foreshock is not a static region; it changes with the ever-changing solar wind conditions. Various kinetic phenomena resulting from variable solar wind conditions interacting with the quasi-parallel bow shock have been both simulated and observed ([Thomsen et al., 1988]; [Paschmann et al., 1988]; [Thomas and Brecht, 1988]; [Schwartz, 1995]; [Sibeck et al., 2002]; [Omidi and Sibeck, 2007]; [Eastwood et al., 2008]). Foreshock phenomena are important as they can result in extreme magnetospheric disturbances ([Jacobsen et al., 2009]; [Turner et al., 2011]) and are features of other planetary systems, with previously reported observations at Venus ([Slavin et al., 2009]), Mars ([Øieroset et al., 2001]), and Saturn (Masters et al., 2009]). Most recently, 2.5-dimensional global hybrid simulations were used to predict a previously unobserved (or previously observed but misclassified) foreshock phenomenon: foreshock bubbles ([Omidi et al., 2010]). Here we present unprecedented, multi-point observations of foreshock bubbles, including the events' global effects on the magnetosphere and the energetic ions and electrons accelerated in the foreshock bubbles via first and second order Fermi and shock drift acceleration processes.

By contrast to magnetohydrodynamic models, hybrid simulations, which treat ions kinetically using particle-in-cell methods and electrons as a massless fluid, can be used to predict a wide variety of structures generated by wave-particle interactions upstream of the bow shock. As predicted with hybrid simulations ([Omidi et al., 2010]), foreshock bubbles (FBs) form due to kinetic interactions between suprathermal, backstreaming ions and incident solar wind plasma with embedded IMF discontinuities moving through and altering the ion foreshock. IMF discontinuities causing a deflection and gyration of the backstreaming ion beam result in the formation of a density and field depletion region with temperatures up to several orders of magnitude hotter than the upstream plasma, highly deflected and sometimes sunward flows, and ultra-low frequency (ULF) wave activity forming the core of the FB (see Fig. 1c). This core is bounded by

denser plasma exhibiting deflected flows and enhanced field strength. FB core plasma acts as a barrier to upstream solar wind and results in the formation of a fast magnetosonic shock wave at its upstream edge, which is also part of the FB structure (see Fig. 1c). FBs can form for a variety of IMF orientations, but FBs can only impact the magnetosphere when they form on the dayside, i.e., when the angle between the IMF and solar wind velocity is small (~45 degrees or less). Transverse to the solar wind velocity direction, FBs scale with the width of the ion foreshock (i.e., 10's of Earth radii, R_E, at Earth). Parallel to the velocity direction, they grow in time and can be on the order of 10 R_E at Earth. FBs convect with the solar wind, i.e., primarily in the negative X_{GSM} direction. A spacecraft observing a FB from the foreshock would observe the core first, with its deflected flows, depressed density and field strength, and increased temperatures, followed by the shock wave exhibiting strong increases in density and field strength, but the IMF discontinuity responsible for the event may become indistinguishable in the enhanced ULF waves in the original foreshock and core (see supplementary material). When FBs impact the magnetosphere, the density cavity in the core results in magnetopause expansion, and the shock results in compression. Effects from these changes should be observable in field measurements throughout the magnetosphere. Finally, FBs should be efficient particle accelerators via 1st and 2nd order Fermi and shock drift acceleration processes.

Observations of FBs may have previously been mistaken for hot flow anomalies (HFAs) ([Thomsen et al., 1988]; [Paschmann et al., 1988]; [Omidi and Sibeck, 2007]; [Eastwood et al., 2008]), as they share many similar features, including relation to IMF discontinuities, hot core temperatures, density and field depletions, deflected solar wind flows, shocks or compression regions bounding at least one side, and *in situ* observation times of ~1 to several minutes ([Facsko et al., 2008]). Current theory suggests that HFAs form when suprathermal ions in the foreshock are guided and focused along an IMF discontinuity by electric fields on one or both sides of the discontinuity. When this occurs, the temperature and thermal pressure are greatly enhanced at a finite region around where the discontinuity intersects the bow shock. This drives thermal plasma out of this region to maintain pressure balance, resulting in depressed field strengths and densities. This ejected plasma piles up at the edges of HFAs resulting in compression regions, which may form into shocks depending on the HFA geometry and motion with respect to the

incident solar wind. Despite these similarities, HFAs and FBs form independently and have distinct differences. HFAs are transient features that form and move along the bow shock at the intersection point between the bow shock and a discontinuity in the IMF. Thus, their motion (and observation time) is fully dependent on the orientation of the discontinuity with respect to the local bow shock. Based on simulations ([Schwartz, 1995], [Omidi and Sibeck, 2007]), HFAs along Earth's bow shock should only be on the order of ~1 R_E in size both along the bow shock and normal to it. Considering the similarities between HFAs and FBs observed *in situ*, care must be taken using multi-spacecraft observations to distinguish between the two. Key differences are: 1) HFA formation requires an IMF discontinuity be connected to the bow shock but FB formation does not; 2) FBs can be 10 R_E or more in size and can form far upstream of the bowshock but HFAs form at the bow shock and are on the order of only a few R_E; 3) FBs convect with the solar wind but HFAs move with the discontinuity along the bow shock; HFAs require 4) the electric field on one or both sides of the discontinuity to be pointed back into it and 5) fast solar wind speed (>425 km/s), but FBs have no such requirements.

We employ observations from NASA's Time History of Events and Macroscale Interactions during Substorms (THEMIS) mission ([Angelopoulos et al., 2008]), consisting of five identically instrumented spacecraft that were launched in early 2007 and an extensive network of ground-based observatories. Also included here are observations from the National Oceanic and Atmospheric Administration's GOES spacecraft in geosynchronous Earth orbit (GEO). Figure 1 shows the spacecraft locations at 21:50 UT on Bastille Day (14 July) 2008, just a few minutes prior to the observations of the foreshock bubble and its impact on the magnetosphere. THEMIS-B (TH-B) is upstream of the bow shock on the afternoon-dayside, near apogee, at a radial distance of ~27 R_E, and TH-C is in the same sector though closer to the average bow shock location ([Fairfield, 1971]) at ~19 R_E. Based on the IMF direction and presence of suprathermal ion observations from both spacecraft at 21:50, TH-B and -C are in the quasi-parallel shock region, i.e. foreshock, at this time. TH-D and -E are at a radial distance of ~11.5 R_E each and along the afternoon magnetopause; they are both inside the magnetosphere and within 1 R_E of the model magnetopause location ([Shue et al. 1997]) calculated using the TH-B observations. TH-A is in the inner-magnetosphere and is

not used here. GOES-10, -11 and -12 are at GEO in the afternoon local time sector during the period of interest, and the GOES-11 and -10 sub-satellite points on Earth flank North America.

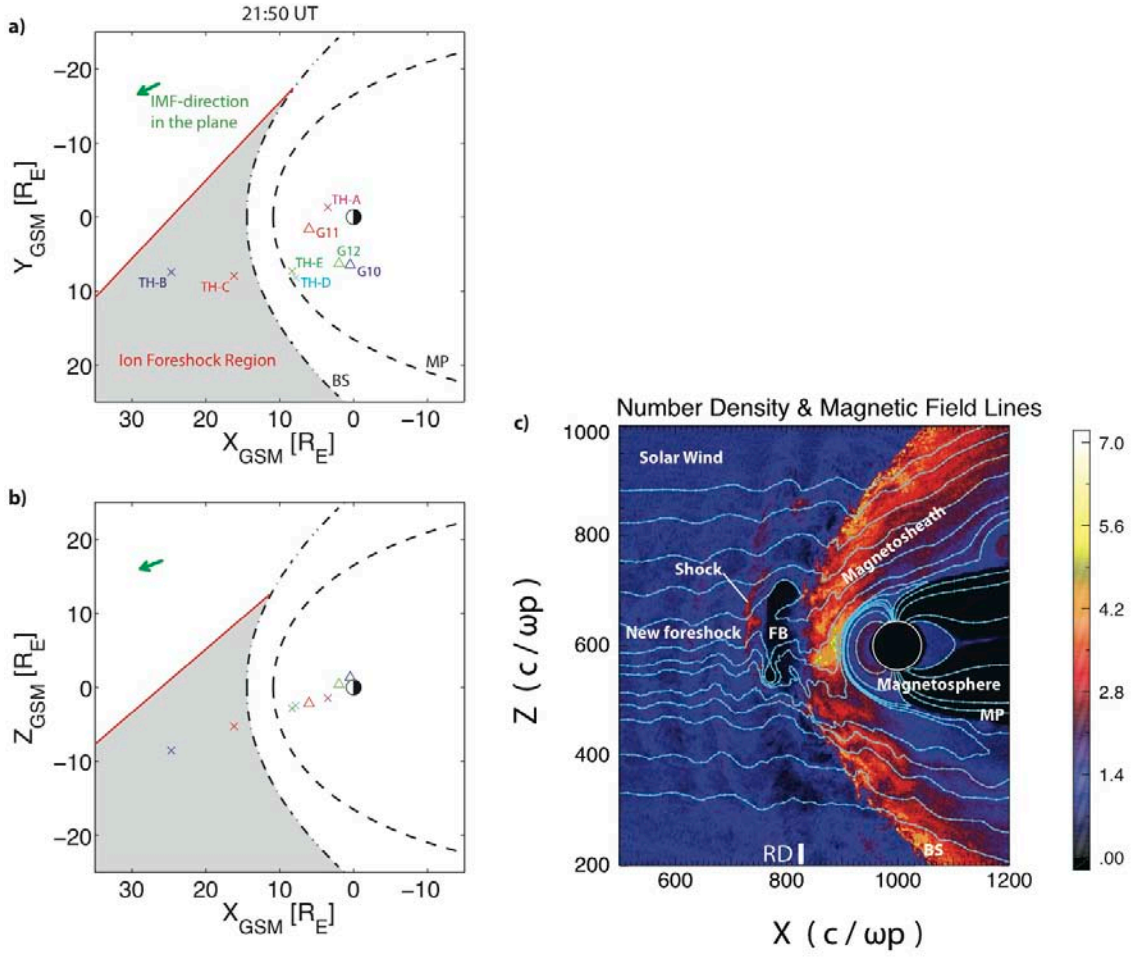

Figure 1: a) and **b)** THEMIS and GOES locations at 21:50 UT on 14 July 2008. Magnetopause (MP) and bow shock (BS) models ([Shue et al, 1997], [Fairfield, 1971]) are shown with the dashed lines. Note that North America spans from pre-noon to post-dusk (+X, +Y quadrant) at this time. The shaded gray region shows the estimated ion foreshock region, and the green arrows show the IMF direction in each plane. **c)** 2.5-dimensional hybrid simulation results of a foreshock bubble ([Omidi et al., 2010]) showing number density in color, normalized to the solar wind, and magnetic field lines. The X and Z axes are in units of the ion skin depth, where c is the speed of light and ω_p is the ion plasma frequency. The axes are in simulation coordinates where the origin is located at the lower left corner of the simulation box. The white circle around the Earth represents the simulation's inner boundary, which is a dipole inside a perfectly conducting sphere. The foreshock region here is originally upstream of the subsolar point, since the IMF in the simulation is primarily in the X-direction. Note the wave activity in this region, which is a typical feature of the ion foreshock and is evident in both the density and the magnetic field lines. A rotational discontinuity (RD) in the IMF is indicated on the figure and results in the formation of a foreshock bubble (FB), which is the large density depletion region around the subsolar point. The shock wave associated with the FB is apparent in the enhanced density band at the upstream edge of the bubble. Note also that the field directions within the bubble can become highly distorted.

Figure 2 shows the TH-B and -C observations from the period of interest. The features observed by TH-C centered around 21:58 UT are those we primarily focus on here. Starting at ~21:57:35 UT, the field strength drops and the ion and electron densities drop rapidly, while their temperatures increase rapidly. The solar wind velocity actually reverses direction, with a positive V_X component indicating sunward flows from 21:57:48-21:58:06 UT. The Y and Z components of the velocity are both enhanced through this encounter, with strong positive V_Y and negative V_Z both greater than 200 km/s, which is typical for magnetosheath deflections based on the spacecraft location (Fig. 1). The solar wind beam of ions is dispersed, and there is an enhancement of several orders of magnitude for fluxes of energetic (E >1 keV) electrons. This encounter culminates in a shock observed between 21:58:12 and 21:58:20 UT. The shock exhibits very strong magnetic field strength (peaking at ~28 nT), density (>10 cm^{-3}), and greatly enhanced total pressure (>10x the ambient solar wind pressure). These features observed by a single spacecraft would be best interpreted as those of an HFA, since central density and field strength dropouts, temperature enhancements, deflected solar wind flows, and shocks on either one or both boundaries are all characteristic observations of HFAs near planetary bow shocks. However, the feature in question here is also observed more than 8 R_E upstream at TH-B between 21:56:06 and 21:57:36. A timing analysis between the two spacecraft confirms that this feature is convecting with the solar wind at ~630 km/s and thus not moving along the bow shock. TH-B's encounter also reveals the size scale of this feature in the X_{GSM} direction to be ~9 R_E. Interestingly, the features observed by TH-C between 21:55:47 and 21:56:38 UT, revealing depressed field strength and densities, enhanced temperatures and energetic ions and electrons, and deflected solar wind flows, are also consistent with field and density dropouts and temperature increases observed around 90 seconds prior at TH-B, which is approximately the same amount of time the solar wind takes to travel between the two spacecraft. Furthermore, the velocity deflection observed by TH-B just before 21:56 UT is primarily in the negative Y_{GSM} direction, which reveals that this deflection is not related to the bow shock since it is inconsistent with the geometry. Summarizing, these events: 1) are independent of the bow shock, 2) are approximately 9 R_E in size in the X_{GSM} direction, and 3) are convected by the solar wind; each of these features are inconsistent with the expected results for HFAs (see additional details in the supplementary material) and consistent with those for FBs, revealing that at least two of these events occurred during this period.

i-a)

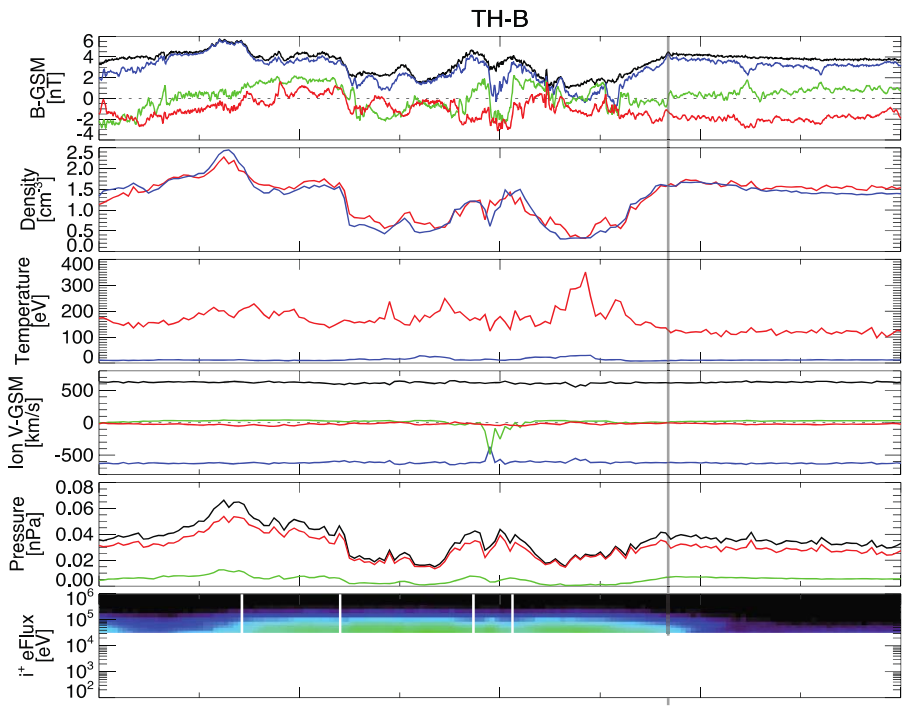

ii-a)

b)

c)

d)

e)

f)

g)

↑ ↑ ↑

Figure 2: TH-B and -C observations during the period of interest. For both TH-B (**i-**) and TH-C (**ii-**): **a)** shows the magnetic field components in GSM (XYZ in blue, green, red) and the total field strength (black). **b)** and **c)** show the ion (red) and electron (blue) density and temperature, respectively. Note that for TH-B the scales for these and the pressures are linear, while they are logarithmic for TH-C. **d)** shows the velocity components in GSM (XYZ in blue, green, red) and the speed (black). **e)** shows the plasma thermal (red) and magnetic (green) pressures and their sum (black). **f)** and **g)** show the high and low energy ion (as measured by two different instruments, SST and ESA) and ESA electron flux spectrograms. The numbered regions indicated by the gray vertical lines indicate the three possible foreshock bubbles observed during this period. The arrows at the bottom of the figure point to the times (21:55:47, 21:56:38, and 21:58:17 UT) mentioned in the text for various enhancements observed at TH-C. These events as observed by TH-C are consistent with those expected for foreshock bubbles ([Omidi et al., 2010]), and similar, though less extreme, features are observed nearly 10 R_E upstream approximately 1.5 minutes before by TH-B, which is consistent with these events convecting with the solar wind, eliminating the possibility that they are hot flow anomalies.

To study the effects the FBs have on the magnetosphere, we examine TH-D and -E, GOES, and THEMIS ground magnetometer observations. Figure 3 shows the data from TH-D and 2 ground magnetometers. TH-D observes six distinct magnetopause crossings, the timing of which approximately corresponds with the propagation time for the pressure, density, and field enhancements observed by TH-C at 21:55:47, 21:56:38, and 21:58:17 UT, the last of which is the shock upstream of the FB observed by TH-C around 21:58 UT. The periods before these crossings reveal velocity components in the positive normal direction (in the LMN boundary normal coordinate system, see supplementary material), which is indicative of magnetopause expansion that would result in response to the low density in the core of FBs. Deeper within the magnetosphere, the effect of the FBs is also observed and propagates from noon towards the magnetotail, further evidence that the feature is convecting with the solar wind. GOES observations confirm the tailward motion of the compressional waves associated with the magnetospheric motion resulting from these events (see supplementary material). On the ground, magnetometers across North America also observed the feature propagating eastward, which is tailward since the continent is in the afternoon local time sector at this time. Also, there is a latitudinal dependence on the response; the stations at higher latitudes observe a larger amplitude field change. This reveals that FBs impacts on the magnetosphere affect field-aligned and ionospheric currents, similar to other transient magnetopause events. Interestingly, the Whitehorse observations best match the conditions observed by TH-C. The strong negative bays in the H component correspond to the magnetosphere expanding, while positive enhancements in this component imply magnetospheric compression. Thus, the peaks observed at 21:55:40, 21:56:50, and 21:59:30 UT result from the above-mentioned pressure, density, and field

enhancements observed by TH-C, and the negative bays prior to these features result from the magnetopause expansion in response to the density depletion in the FBs. These observations confirm that foreshock bubbles result in global magnetospheric disturbances.

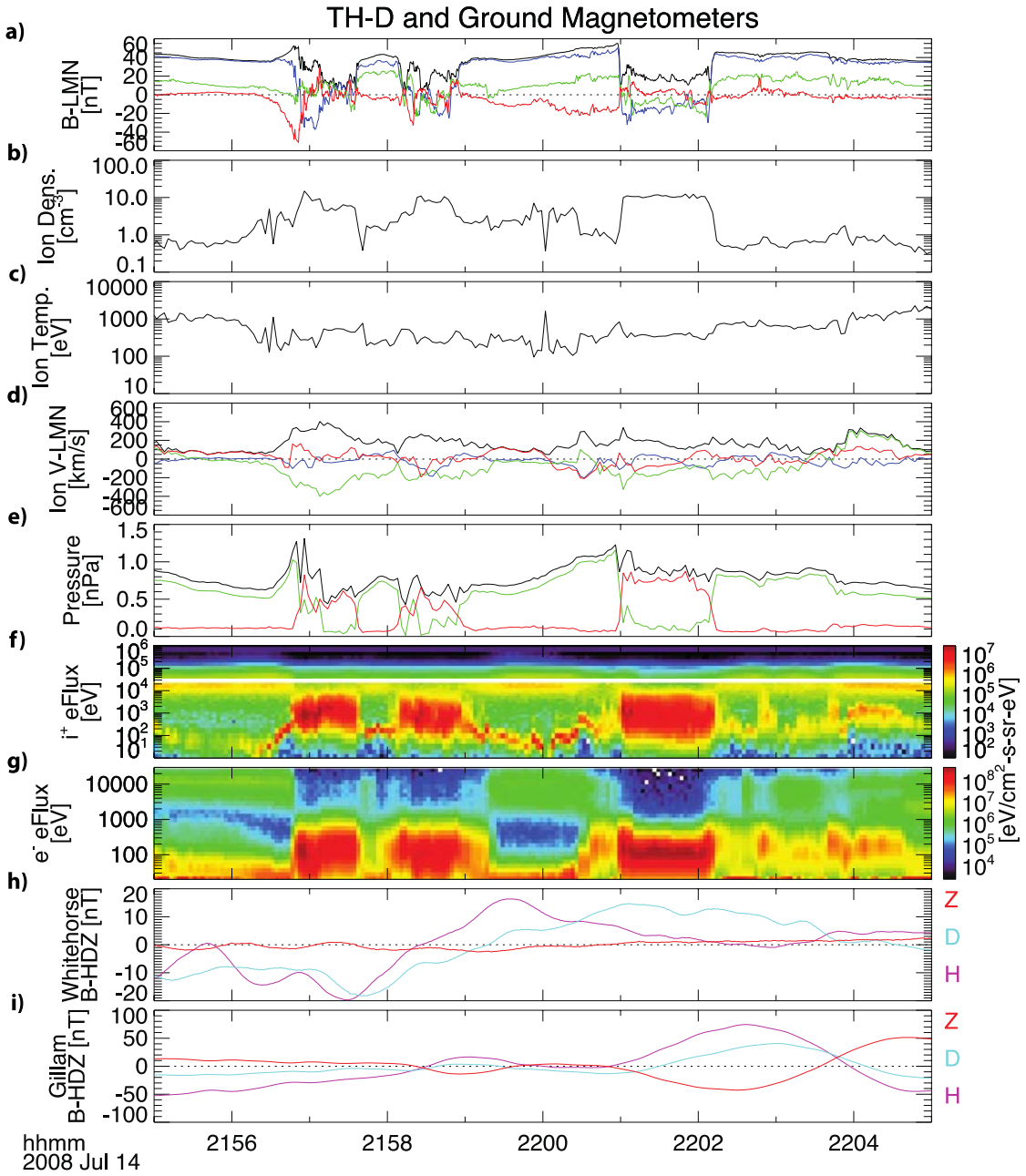

Figure 3: TH-D observations along the magnetopause from 21:55-22:05 UT; note that **a) – g)** correspond to the same quantities shown in Figure 2. **h) - i):** THEMIS ground magnetometer observations of field variations with the long-term average subtracted. Whitehorse is located at magnetic latitude and longitude of 63.66 and 278.14 degrees, respectively. Gillam is located at 66.18 and 332.78 degrees. The coordinate system is HDZ, where H is positive northward, D is positive westward, and Z is positive up from the

ground station. Note, these plots are for a different time period than shown in Figure 2, from 21:55 – 22:05 UT.

FBs are associated with two shocks: the original shock responsible for the foreshock formation (e.g., Earth's bow shock) and the shock that forms at the outer layer of FBs, and these shocks converge on each other as the FBs are convected with the upstream plasma. Furthermore, the presence of ULF wave activity results in enhanced particle scattering and reflections. Thus, FBs create an ideal situation for both first and second order Fermi acceleration and shock drift acceleration of solar wind and foreshock particles ([Scholer et al., 1998], [Giacalone, 1992], [Omidi et al., 2010]). From Figure 2, both the ion and electron fluxes are enhanced at higher energies, up to ~200 keV for ions and ~10 keV for electrons, during this period. The electron enhancements are most clearly restricted by the core bubble regions, and the fluxes at E between 0.5 and 10 keV are enhanced by around two orders of magnitude. Since collisionless shocks in magnetized plasmas are known to occur throughout the Universe (e.g., Earth's and other planetary bow shocks, the heliospheric bow shock and those around other stars, and supernovae), FBs should occur at quasi-parallel shocks where the upstream magnetic field exhibits discontinuous behavior. Net particle acceleration relates to the system scale size, the converging shocks' relative velocity, and incident particle distributions. The observations presented here (see also particle distribution slices and flux energy spectra in the supplementary material) provide direct measurements of both ions and electrons accelerated by converging shocks in FBs at Earth's foreshock, and these can be used to constrain models to estimate energetic particle generation by FBs at other shocks throughout the Universe.

References and Notes:

1. M. Scholer, H. Kucharek, and K. J. Trattner, Injection and acceleration of energetic particles at collisionless shocks, *Adv. Space Res.*, **21**, 533 (1998).
2. J. Giacalone, Shock drift acceleration of energetic protons at a planetary bow shock, *J. Geophys. Res.*, **97**, 8307 (1992).
3. S. A. Fuselier, Ion distributions in the Earth's foreshock upstream from the bow shock, *Adv. Space Res.*, **15**, 43 (1995).
4. D. G. Sibeck, N. Omidi, I. Dandouras, and E. Lucek, On the edge of the foreshock: model-data comparisons, *Ann. Geo.*, **26**, 1539 (2008).
5. M. F. Thomsen, J. T. Gosling, S. J. Bame, and K. B. Quest, On the origin of hot diamagnetic cavities near the Earth's bow shock, *J. Geophys. Res.*, **93**, 11311 (1988).

6. G. Paschmann, G. Haerendel, N. Sckopke, E. Mobius, H. Luhr, and C. W. Carlson, Three-dimensional plasma structures with anomalous flow directions near the Earth's bow shock, *J. Geophys. Res.*, **93**, 11279 (1988).
7. S. J. Schwartz, Hot flow anomalies near the Earth's bow shock, *Adv. Space Res.*, **15**, 107 (1995).
8. N. Omidi and D. G. Sibeck, Formation of hot flow anomalies and solitary shocks, *J. Geophys. Res.*, **112**, A10203 (2007).
9. J. P. Eastwood, D. G. Sibeck, V. Angelopoulos, T. D. Phan, S. D. Bale, J. P. McFadden, C. M. Cully, S. B. Mende, D. Larson, S. Frey, C. W. Carlson, K.-H. Glassmeier, H. U. Auster, A. Roux, and O. Le Contel, THEMIS observations of a hot flow anomaly: Solar wind, magnetosheath, and ground-based measurements, *Geophys. Res. Lett.*, **35**, L17S03 (2008).
10. V. A. Thomas and S. H. Brecht, Evolution of diamagnetic cavities in the solar wind, *J. Geophys. Res.*, **93**, 11341 (1988).
11. D. G. Sibeck, T. D. Phan, R. Lin, R. P. Lepping, and A. Szabo, Wind observations of foreshock cavities: A case study, *J. Geophys. Res.*, **107**, 1271 (2002).
12. K. S. Jacobsen, T. D. Phan, J. P. Eastwood, D. G. Sibeck, J. I. Moen, V. Angelopoulos, J. P. McFadden, M. J. Engebretson, G. Provan, D. Larson, and K.-H. Fornacon, THEMIS observations of extreme magnetopause motion caused by a hot flow anomaly, *J. Geophys. Res.*, **114**, A08210 (2009).
13. D. L. Turner, S. Eriksson, T. D. Phan, V. Angelopoulos, W. Tu, W. Liu, X. Li, W.-L. Teh, J. P. McFadden, and K.-H. Glassmeier, Multispacecraft observations of a foreshock-induced magnetopause disturbance exhibiting distinct plasma flows and an intense density compression, *J. Geophys. Res.*, **116**, A04230 (2011).
14. J. A. Slavin, M. H. Acuna, B. J. Anderson, S. Barabash, M. Benna, S. A. Boardsen, M. Fraenz, G. Gloeckler, R. E. Gold, G. C. Ho, H. Korth, S. M. Krimigis, R. L. McNutt Jr., J. M. Raines, M. Sarantos, S. C. Solomon, T. Zhang, and T. H. Zurbuchen, MESSENGER and Venus Express observations of the solar wind interaction with Venus, *Geophys. Res. Lett.*, **36**, L09106 (2009).
15. M. Øieroset, D. L. Mitchell, T. D. Phan, R. P. Lin, and M. H. Acuna, Hot diamagnetic cavities upstream of the Martian bow shock, *Geophys. Res. Lett.*, **28**, 887 (2001).
16. A. Masters, H. J. McAndrews, J. T. Steinberg, M. F. Thomsen, C. S. Arridge, M. K. Dougherty, L. Billingham, S. J. Schwartz, N. Sergis, G. B. Hospodarsky, and A. J. Coates, Hot flow anomalies at Saturn's bow shock, *J. Geophys. Res.*, **114**, A08217 (2009).
17. N. Omidi, J. P. Eastwood, and D. G. Sibeck, Foreshock bubbles and their global magnetospheric impacts, *J. Geophys. Res.*, **115**, A06204 (2010).
18. G. Facsko, K. Kecskemety, G. Erdos, M. Tatrallyay, P. W. Daly, and I. Dandouras, A statistical study of hot flow anomalies using Cluster data, *Adv. Space Res.*, **41**, 1286 (2008).
19. V. Angelopoulos, D. G. Sibeck, C. W. Carlson, J. P. McFadden, D. Larson, R. P. Lin, J. W. Bonnell, F. S. Mozer, R. Ergun, C. Cully, K.-H. Glassmeier, U. Auster, A. Roux, O. LeContel, S. Frey, T. D. Phan, S. Mende, H. Frey, E. Donovan, C. T. Russell, R. Strangeway, J. Liu, I. Mann, J. Rae, J. Raeder, X. Li, W. Liu, H. J. Singer, V. A. Sergeev, S. Apatenkov, G. Parks, M. Fillingim, J. Sigwarth, First results from the THEMIS mission, *Space Sci. Rev.*, **141**, 453 (2008).
20. D. H. Fairfield, Average and unusual locations of Earth's magnetopause and bow shock, *J. Geophys. Res.*, **76**, 6700 (1971).
21. J.-H. Shue, J. K. Chao, H. C. Fu, C. T. Russell, P. Song, K. K. Khurana, and H. J. Singer, A new functional form to study the solar wind control of the magnetopause size and shape, *J. Geophys. Res.*, **102**, 9497 (1997).

Acknowledgments:

N. Omidi acknowledges NSF grant AGS-1007449. We would like to thank the entire THEMIS team and especially the following people for providing various instrument data: Karl-Heinz Glassmeier (spacecraft magnetometers), Jim McFadden (ESA), Davin Larson (SST), and Chris Russell (ground magnetometers). We also thank Howard Singer and NASA's CDAWeb database for free online access to the GOES magnetometer data. This work was funded under NASA contract NAS5-02099.

Author Contributions: D. L. Turner conducted the majority of data analysis for this study. N. Omidi provided simulation results and expertise on foreshock bubbles. D. G. Sibeck provided expertise on foreshock observations and phenomena. V. Angelopoulos provided the THEMIS data and expertise on its use.

Supplementary Material for

First Observations of a Foreshock Bubble at Earth: Implications for Magnetospheric Activity and Energetic Particle Acceleration

Drew L. Turner[1], Nick Omidi[2], David G. Sibeck[3], and Vassilis Angelopoulos[1]

[1] University of California, Los Angeles, CA, USA
[2]Solana Scientific Inc., Solana Beach, CA, USA
[3]NASA Goddard Space Flight Center, Greenbelt, MD, USA

Correspondence to: drew.lawson.turner@gmail.com

This file includes:

Materials and Methods

THEMIS Dataset

NASA's Time History of Events and Macroscale Interactions during Substorms (THEMIS) mission currently consists of three (five originally), identically instrumented spacecraft in highly eccentric orbits near the magnetic equatorial plane [Angelopoulos, 2008]. THEMIS also incorporates an extensive network of ground magnetometers throughout Canada and Alaska. For this study, we use THEMIS solid state telescope (SST) energetic ion data, electrostatic analyzer (ESA) plasma data ([McFadden et al., 2008]), fluxgate magnetometer (FGM) data ([Auster et al., 2008]) from THEMIS-B (TH-B), -C, -D, and -E as well as the ground station magnetometer data ([Russell et al., 2008]). We retrieved and processed these data using the THEMIS Data Analysis Software (TDAS) tools. For the SST ion data, sunlight contamination has been removed. From the ion and electron densities from ESA shown in Figure 2, the good agreement between the species indicates that the instruments captured the narrow solar wind beam ensuring accurate plasma moments.

GOES Dataset

NOAA's Geostationary Operational Environment Satellites (GOES) are primarily for monitoring terrestrial weather, however, they have been equipped with space environment monitors such as magnetometers, X-ray sensors, and energetic particle instruments. Here we use the high-resolution fluxgate magnetometer data available at NASA's CDAWeb: <http://cdaweb.gsfc.nasa.gov>. Additional details on the GOES instrumentation and spacecraft can be found online at: <http://www.ngdc.noaa.gov/stp/satellite/goes/index.html>.

Additional Study Details

Boundary Normal Coordinates and Additional Details of Magnetopause Disturbance:

The boundary normal coordinate system [Russell and Elphic, 1978] is useful for magnetopause studies and interpretation of observations near the magnetopause. In this right-handed, orthonormal system, the L-direction is in the direction of the expected magnetic field just inside of the magnetopause; it corresponds closely to the Z_{GSM} direction. The N-direction is normal to the local magnetopause and is positive outward. The M-direction completes the system, and it is positive in the sunward (anti-sunward) direction on the dusk (dawn) side of the magnetosphere.

Examining in more detail the TH-D and -E (see Figure S2) observations of the magnetopause disturbances associated with these FBs, some interesting features include: the distorted fields and high pressure at the first magnetopause crossing, the very fast sheath flows (~600 km/s) observed by TH-E after the first magnetopause crossing, TH-D observing more magnetopause crossings than TH-E, and evidence of the large shock before 22:01 UT. First considering the highly distorted fields and high pressures observed by both spacecraft during the first magnetopause crossing between 21:56 and 21:57 UT, there are ion energy flux signatures consistent with rapid magnetopause motion just prior to the magnetopause crossings, which are consistent with those discussed in previous works [e.g., Savaud et al., 2001; Turner et al., 2011]. The crossings themselves reveal fields with very strong normal components, indicating significant curvature along the magnetopause surface. Interestingly, there are bipolar B_N signatures, but these are likely not flux transfer events (FTEs) since the energy fluxes reveal very sudden and distinct transitions from magnetospheric to sheath plasma. In FTEs, it is expected to see mixed plasma from both the magnetosphere and the sheath [e.g., Zhang et al., 2010 and references therein]. Regardless of whether or not these are FTEs, the high pressure is further indication that the fields were highly distorted along the magnetopause, as this pressure is likely balanced by the magnetic tension associated with the curved fields.

Next, the very fast velocity observed by TH-E prior to 21:57 UT is unexpected. When the solar wind crosses the bow shock, it is slowed significantly, by a factor of 4 near the subsolar point based on the Rankine-Hugoniot jump conditions. TH-E has just crossed into the magnetosheath at this time and should still be quite close to the magnetopause, along which the velocity is expected to be slowest. However, TH-

E observes velocity peaking near 600 km/s, which is close to the total velocity in the solar wind upstream of the bow shock observed by TH-B and -C. TH-D observes similarly high flow velocity, around 400 km/s, further downstream. These spacecraft are not located at the subsolar point, but based on the Spreiter et al. [1966] hydromagnetic model, the velocity should be between 0.4 and 0.5 of the solar wind velocity, so both spacecraft are observing faster than expected flows. This is an interesting feature; one explanation may be that it results from plasma jets that form along a highly distorted bow shock [Hietala et al., 2009].

TH-D crosses the magnetopause twice more than TH-E during the period in question. The extra crossings are more consistent with the picture from TH-C of three FBs during this period. Both spacecraft do observe three distinct periods of positive V_N, velocity normal to the magnetopause consistent with outward expansion, which would occur when the low-density core of a FB impacts the magnetopause. However, the presence of additional, localized phenomena in the sheath, like the jets mentioned in the previous paragraph, might explain the difference. Regardless, this reveals that the FBs effects on the magnetopause are complex, with large-scale dynamics on timescales less than a minute and distances less than 1 R_E.

Finally, both spacecraft observed the same shock observed by TH-C at 21:58:17 UT. Note the similar field features, with the strong negative B_L, corresponding to the strong negative B_Z observed at TH-C. This is clear as the distinct plasma region between 22:00:45 and 22:01:00 UT at TH-E and for the briefer period of 22:01:00 ~ 22:00:07 UT at TH-D, which indicates that the shock has diminished rapidly as it evolves in the sheath.

Comparing FB Observations to those from a HFA on the Same Day

It is important to quantify the differences between FBs and HFAs considering their numerous similarities and that FB observations may have been mistaken for HFAs in the past. Figures S3 and S4 show TH-B solar wind observations and TH-C observations of a HFA on the same day as the observations of the FBs (14 July 2008). Figure S3 shows upstream observations by TH-B, and there are two IMF discontinuities during this period: the first between 22:27:10 and 22:27:30 UT and the second around 22:28:33 UT. Suprathermal ions and correlated magnetic field strength and density variations, both evidence of the ion foreshock, are evident around the time of the first discontinuity but not during the second. Note that there are no significant temperature or velocity variations associated with either of these, though there are slight enhancements in the suprathermal electron population. Next, observations closer to the bow shock measured by TH-C are shown in Figure S4, which is centered around the observations of a clear HFA. The two discontinuities in the IMF observed upstream from TH-B are seen between 22:28:10 and 22:28:40 UT and 22:29:10 UT, respectively. We calculated a minimum variance analysis for each of these discontinuities to determine their normal directions and propagation times between the two spacecraft. These reveal normal directions of [0.57, -0.59, 0.57] and [0.57, -0.71, 0.41] (both [XYZ] in the GSM coordinate frame) and propagation times of 61 seconds and 72 seconds, respectively for the two discontinuities. The propagation times are similar to those observed (~60 and ~40 seconds, respectively), and the difference (particularly for the second discontinuity) can be attributed to error and additional variation in the plasma between the two spacecraft. The observations by TH-C during the first discontinuity reveal a clear HFA. Centered around the discontinuity are: magnetic field strength and plasma density cavities flanked on both sides by enhanced field strength and density regions, a hot central core, deflected plasma flow, and the presence of suprathermal ions and electrons. These are all classic features of HFAs.

There are some key differences between the FB and HFA observed by TH-B and -C on 14 July 2008. First, TH-B observes evidence of the foreshock in both cases, but only for the FB observations does it observe enhanced temperatures and deflected flows. This is expected based on simulations of both FBs and HFAs [e.g., Omidi et al., 2010; Omidi and Sibeck, 2007], which reveal that these features of HFA cores should not extend as far upstream as TH-B is at the time of the observations. Next, in the FB observation at 21:58 UT, TH-C observes a clear bubble region, consisting of field strength and density depletions, enhanced temperatures up to a couple keV, and sunward plasma velocity, followed by an upstream shock, with field strength >20 nT, density >10 cm^{-3}, and a strong pressure enhancement. Note also that there is no shock or evidence of a compression region on the downstream side of the core bubble features. TH-C's

later observations of the HFA are notably different; it observes two distinct compression regions flanking the core and the first IMF discontinuity. This is consistent with the picture of a HFA core expanding into and compressing the plasma around it as it moves *along the bow shock, not with the solar wind*. These compression regions are not full shocks, as is evident from the continuous variation and low field strength and density peaks compared with pre-event levels. These compression regions can evolve into shocks on one or both sides of HFAs depending on how the HFA is moving along the bow shock with respect to the incident solar wind [e.g., Thomsen et al., 1988]. It is clear that, at least in these cases, the HFA maintains more of a pressure balance than the FB shock. One of the most distinguishable differences is in the energetic electron population associated with each of these events. As previously mentioned, the electrons in the FB are enhanced by over 2 orders of magnitude up to around 10 keV throughout the encounter with the foreshock bubble, ~30 seconds. Though the HFA is associated with some enhanced energetic electron fluxes, the duration (~10 secs), magnitude (less than one order of magnitude), and energy range (up to a couple keV) are all inconsistent with what is observed for the FB. This is because the acceleration mechanisms for the two events are probably quite different. For the FB, the electrons are accelerated by first and second order Fermi and shock drift acceleration mechanisms between the two converging shocks. The scenario is entirely different for the expanding, suprathermal ion cores of HFAs, and the exact mechanism responsible for electron heating in HFAs is still an unanswered question, though wave particle interactions may play a role [Zhang et al., 2010]. One caveat that should be noted here is that the HFA observed by TH-C may still be a "young" HFA, i.e., not fully developed [Zhang et al., 2010]. A fully developed HFA may have a hotter core temperature, more strongly deflected flows, and a shock on one or both sides.

Additional Details for GOES and Ground Magnetometers

GOES and THEMIS ground magnetometer data are shown in Figures S5 and S6. These reveal the compressional wave observed by GOES-10, -11, and -12, which is consistent with the timing of the impact of the shock observed by TH-C shortly after 21:58 UT. Based on the spacecraft locations (see Figure 1), this compressional wave is clearly moving tailward. Figure S6 shows magnetometer measurements from THEMIS ground stations across North America. This clearly reveals the global nature of the disturbances associated with the FBs. Since FBs and other foreshock phenomena occur regularly (i.e., multiple times per day) on the dayside, such features may be important in explaining large-amplitude field-aligned current and ionospheric dynamics that map to the dayside magnetopause.

Kinetic Effects on Particles

Finally, we have examined cuts of the particle distribution functions and the flux-energy spectra for the FB at 21:58 UT and compared these with examples from the HFA discussed above, the ion foreshock, and pristine solar wind. These results are summarized in Figures S7, S8, and S9. In the pristine solar wind, the ion beam is evident opposite to the sun-direction and as the peak in fluxes at around 20 keV. Note that there is no backstreaming population, i.e., moving sunward, in the pristine solar wind. The electrons have no significant suprathermal population and are more isotropic than the ions but still exhibit enhanced PSD in the anti-sunward direction. In the ion foreshock, there is a distinct backstreaming, suprathermal population, evident in the enhanced PSD in the positive V-parallel side of Figure S7 (top row, second column from the left). These are the ions accelerated and reflected from the bow shock counter-streaming into the solar wind. Note from Figure S8 that the suprathermal ion fluxes are enhanced by up to around an order of magnitude compared to the pristine solar wind. The electrons in the ion foreshock are more isotropic and reveal an anisotropy, with more PSD at higher energy in the parallel direction. The foreshock bubble reveals that the ion beam of the solar wind has been dispersed and the PSD and fluxes at high-energy is greater than those of the other three plasmas, including in the HFA, up to >100 keV. The electrons in the foreshock bubble are the most distinct from the other plasmas. They are isotropic and include a very significant suprathermal population. The energy spectra reveal that the electrons from 100 eV to 10 keV are enhanced by up to two orders of magnitude more than those for the other plasmas. This is not the case for the HFA that was observed at 22:28 UT by TH-C. In the HFA, a significant suprathermal ion population exists, but the electron population is similar to that from the ion foreshock.

Additional References

1. Hietala, H., et al., Supermagnetosonic jets behind a collisionless quasiparallel shock, *Phys. Rev. Lett.*, **103**, 245001 (2009).
2. Russell, C. T. and R. C. Elphic, Initial ISEE magnetometer results: Magnetopause observations, *Space Sci. Rev.*, **22**, 681 (1978).
3. Savaud, J.-A., et al., Intermittent thermal plasma acceleration linked to sporadic motions of the magnetopause, first Cluster results, *Ann. Geophys.*, **19**, 1523 (2001).
4. Spreiter, J. R., A. L. Summers, and A. Y. Alksne, Hydromagnetic flow around the magnetosphere, *Planet. Space. Sci.*, **14**, 223 (1966).
5. Zhang, H., et al., Evidence that crater FTEs are initial stages of typical FTEs, *J. Geophys. Res.*, **115**, A08229 (2010).

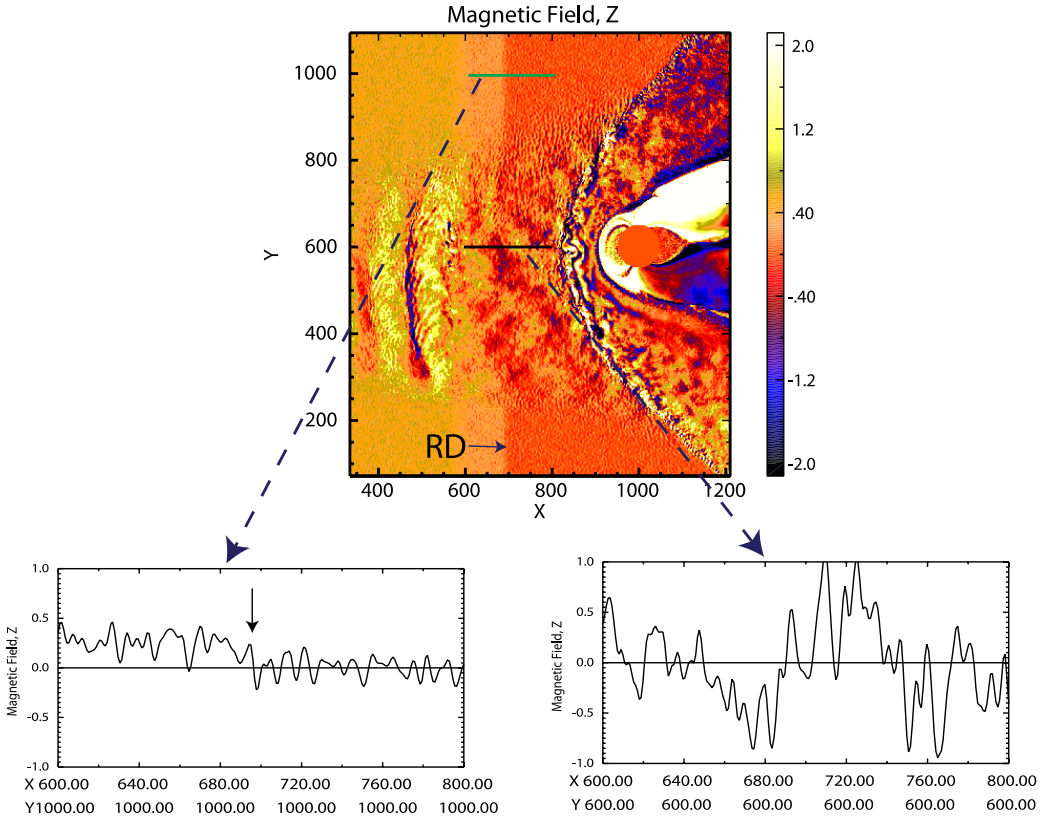

Figure S1: Top: Global hybrid simulation results of a foreshock bubble. Bottom: Line plots of the magnetic field across the rotational discontinuity along the two lines indicated in green (outside of the foreshock) and black (inside the foreshock). These results demonstrate how information of a discontinuity can be lost in the enhanced wave activity in the foreshock.

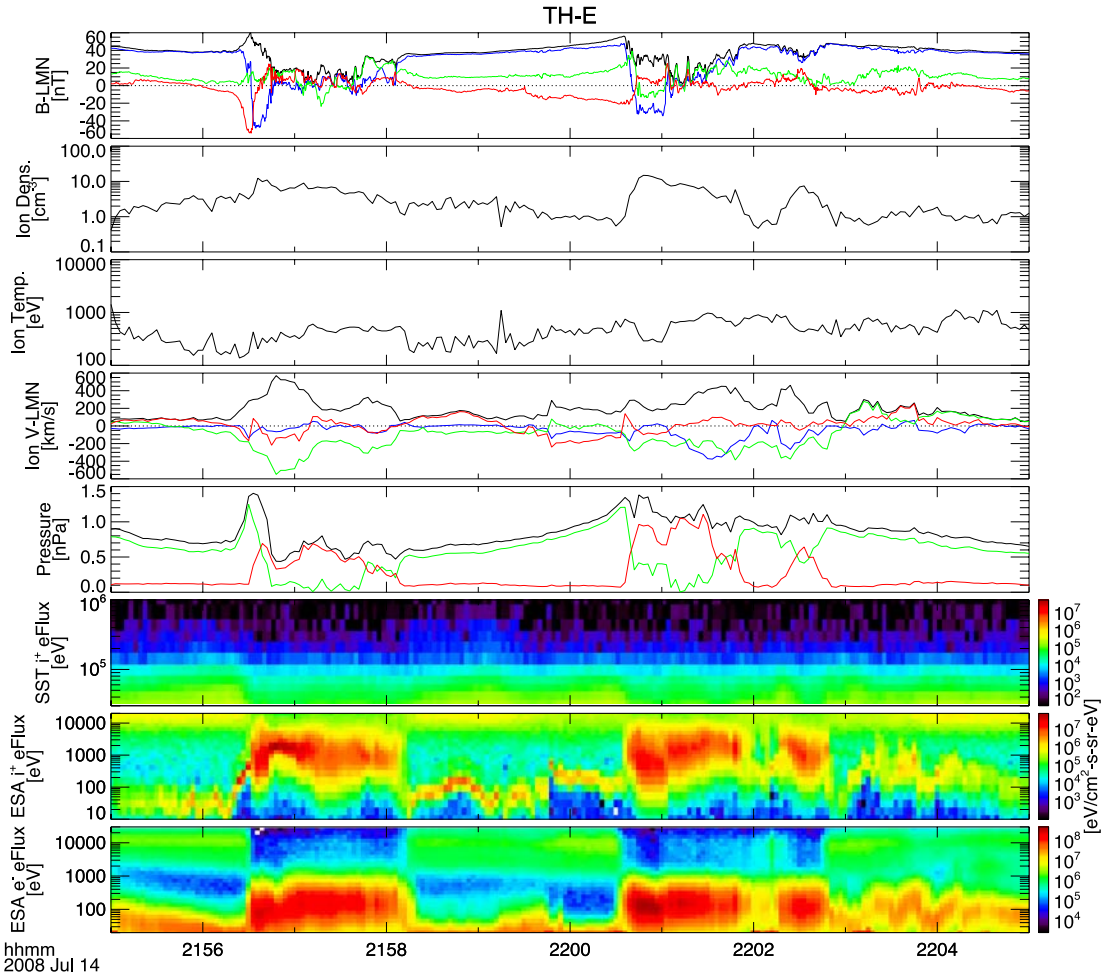

Figure S2: Observations by TH-E during the same period as shown in Figure 3.

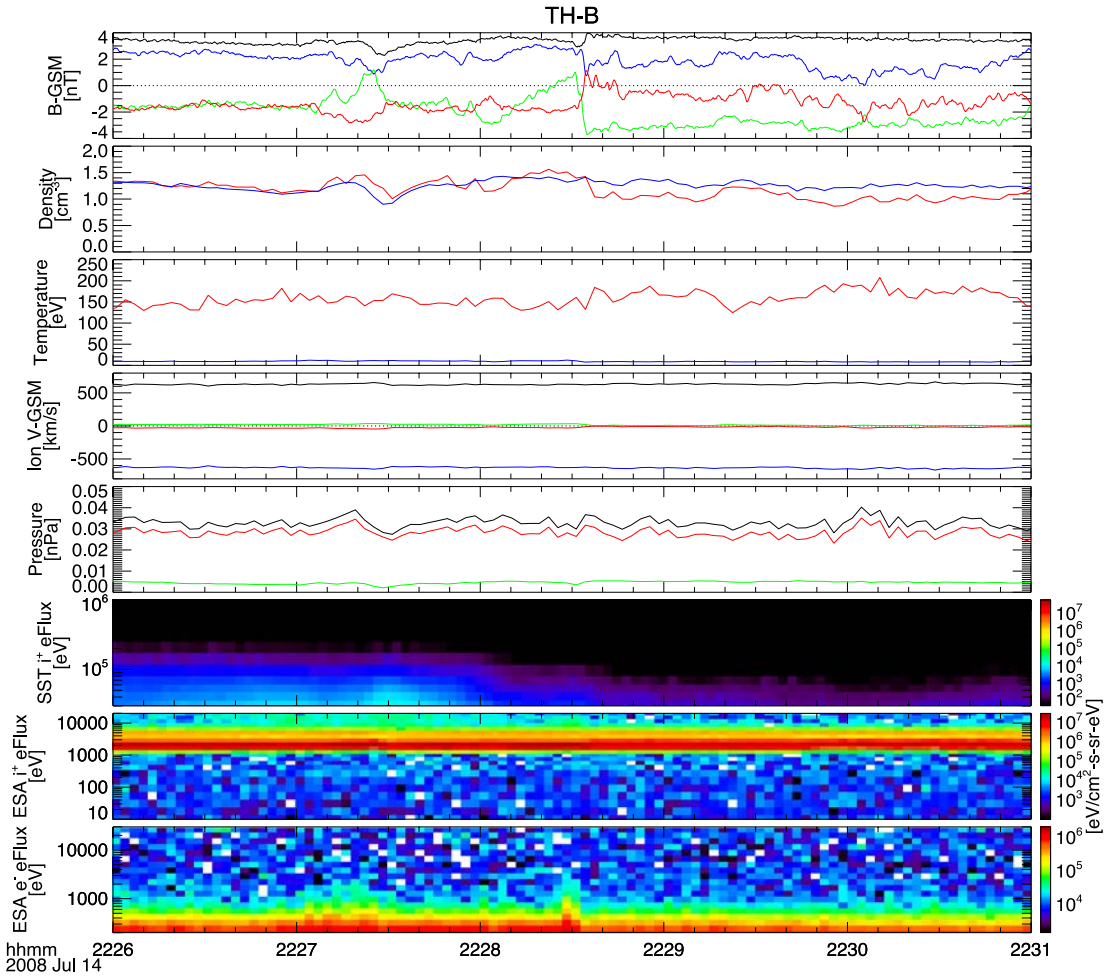

Figure S3: TH-B observations for same time period as when TH-C observes an HFA. Based on a minimum variance analysis to determine IMF discontinuity normal directions, the field changes around 22:27:10 - 22:27:30 UT, which were mostly in B_Y, were most likely responsible for the HFA observed at TH-C one minute later (see Fig. S2). The HFA formation criteria that the –V-cross-B electric field on at least one side of the discontinuity be pointed into the discontinuity was satisfied. Based on the system geometry at this time, the discontinuity had not yet intersected the bow shock.

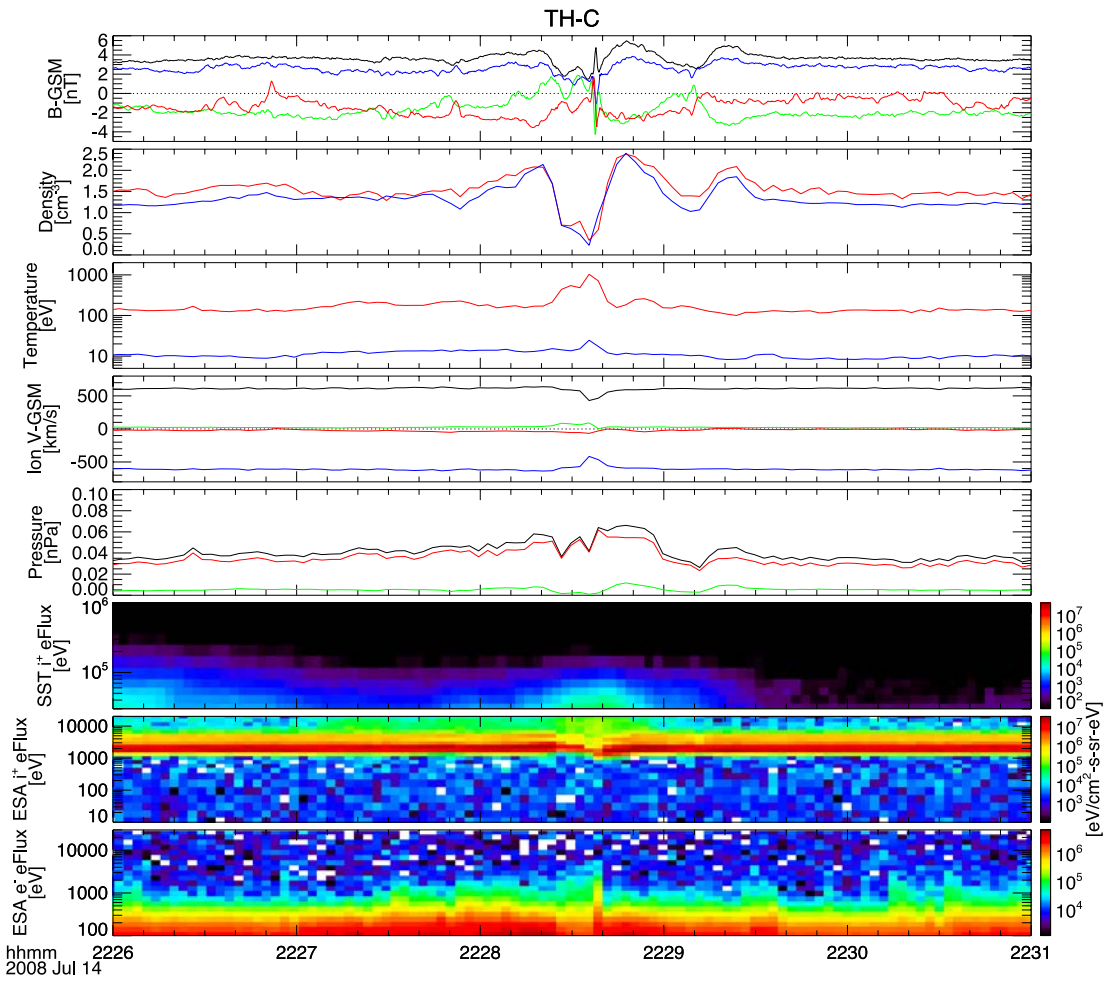

Figure S4: Example of a HFA observed by TH-C on the same day as the FB observations. Note that the field and density reveal "crater-like" features, with a cavity region of depressed field strength and density flanked on either side by compression regions with enhanced field strength and density. The cavity region also exhibits a peak in ion temperature, expected for HFAs. The velocity is slightly deflected, and the ion fluxes reveal an enhancement of the suprathermal population. Interestingly, the energetic electrons seem mostly unaffected, except for the spike at 22:28:38, which also corresponds to a spike in the magnetic field that is not a typical HFA feature.

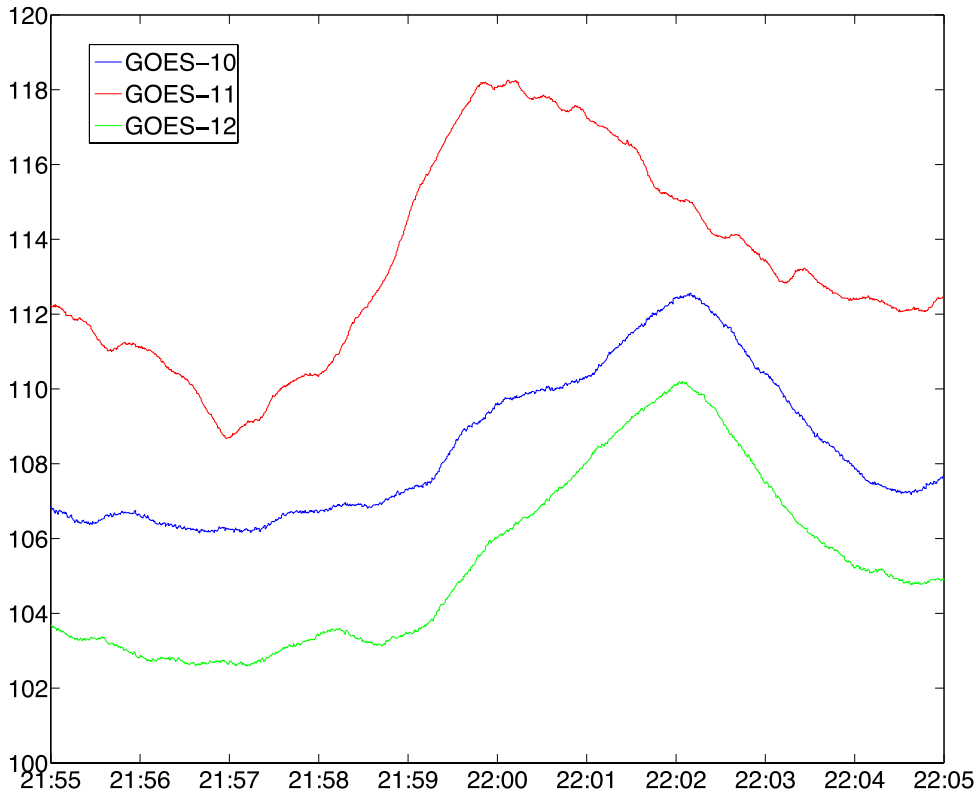

Figure S5: GOES-10, -11, and -12 total magnetic field observations during the events. The strong enhancements indicate a compressional wave in the magnetosphere that is moving tailward.

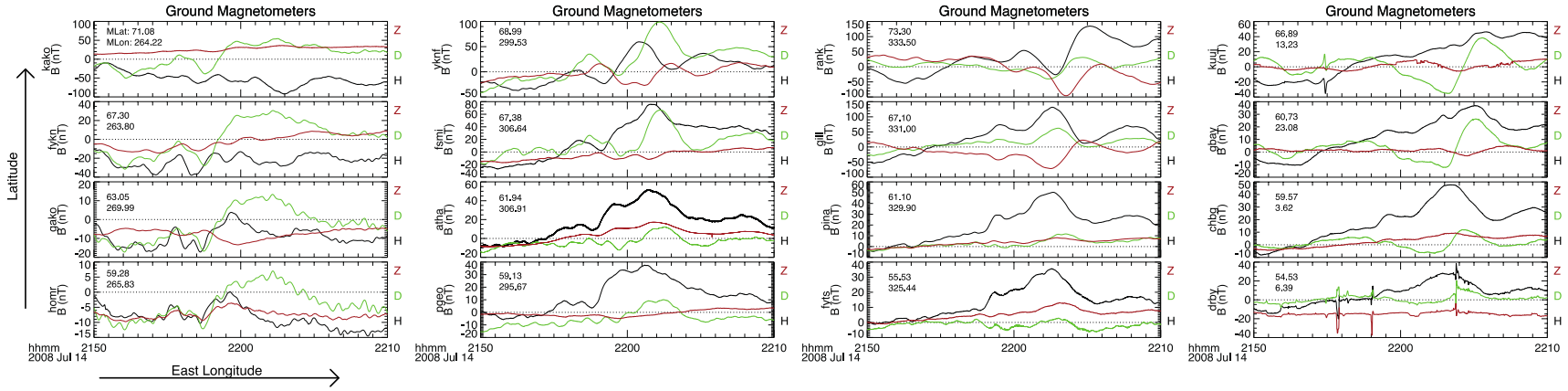

Figure S6: Ground magnetometers from array across Alaska and Canada. Top left (KAKO) is the northern-most station shown from western N. America. The lower rows correspond to lower latitudes and columns to the right correspond to stations further east such that the bottom right (DRBY) is the southern- and eastern-most station shown. Thus, the second and third columns represent western-central and eastern-central longitudinal regions, respectively. The magnetic latitudes and longitudes are displayed for each station in each plots' upper left white space.

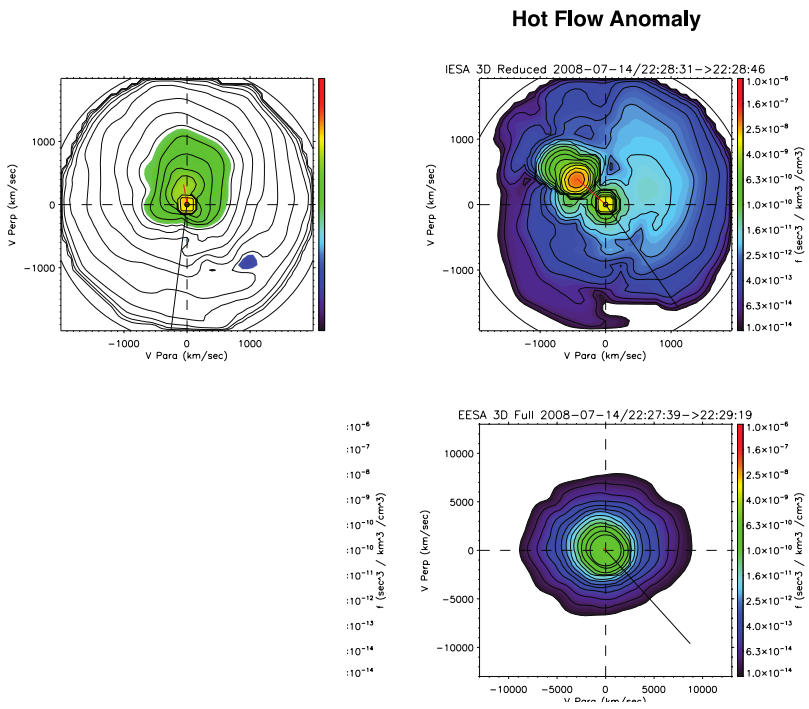

Figure S7: Distribution functions for ions and electrons from TH-C in different plasma regions. The top row is for ions, and the bottom row is for electrons. The columns represent from left to right the distributions from: the pristine solar wind at around 22:50:45 UT, the ion foreshock at around 22:00:00 UT, the foreshock bubble observed at 22:58:00 UT, and the hot flow anomaly observed at 22:28:30 UT. The black line indicates the sun-direction. The red line indicates the peak in phase space density.

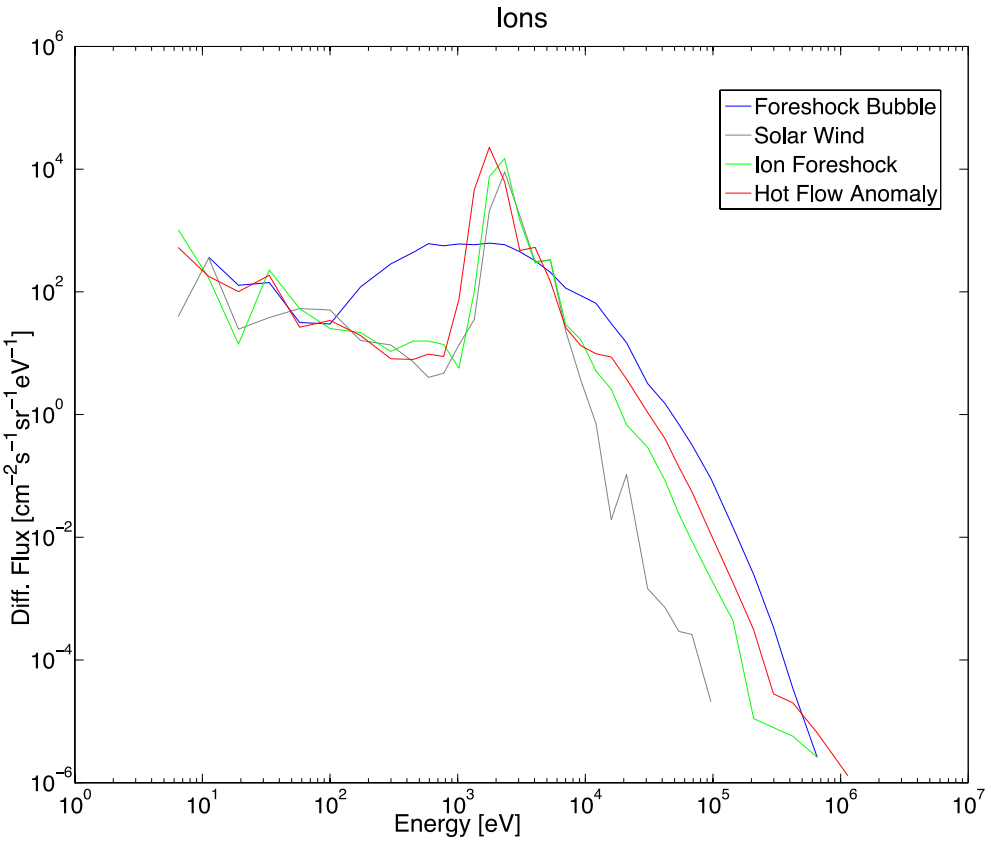

Figure S8: Energy spectra for ion fluxes (SST and ESA combined). The different colored lines show spectra for the same times used in the distribution functions from the different plasma regions in Figure S4.

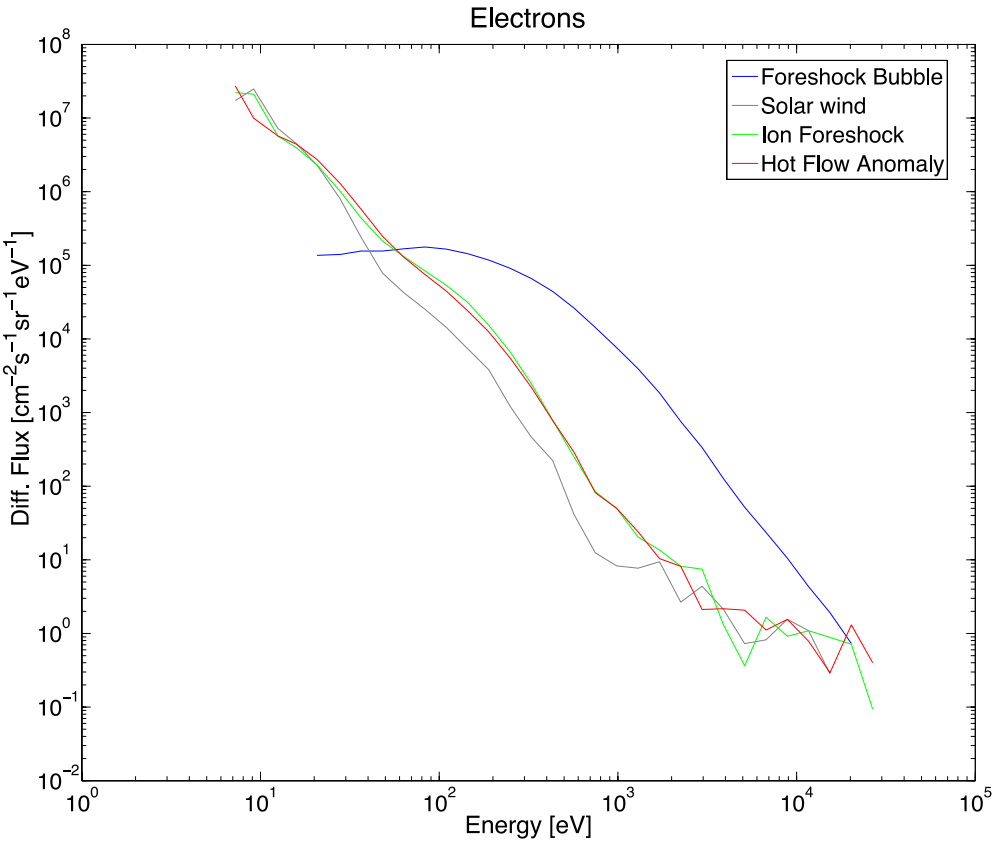

Figure S9: Energy spectra for electron fluxes (ESA only). The different colored lines show spectra for the same times used in the distribution functions from the different plasma regions in Figure S4.